Materials Science and Engineering A 408 (2005) 303–308

www.elsevier.com/locate/msea

Distribution and prediction of solute in Al–Zn–Mg alloys

J. Soto [a], G. Aramburo [b], C. Gonzalez [b], J. Genesca [b], R. Herrera [c], J.A. Juarez-Islas [a,*]

[a] *Instituto de Investigaciones en Materiales, Circuito Exterior s/n, Cd. Universitaria, 04510 México, D.F. Mexico*
[b] *Facultad de Química, Circuito Exterior s/n, Cd. Universitaria, 04510 México, D.F. Mexico*
[c] *Instituto de Física, Circuito Exterior s/n, Cd. Universitaria, 04510 México, D.F. Mexico*

Received in revised form 9 August 2005; accepted 10 August 2005

Abstract

The distribution of solute in α-Al matrix of directionally solidified Al–5.3 at.% (12 wt.%) Zn master alloy with additions of 5.5–11.5 at.% (4.6–9.2 wt.%) Mg was determined and predicted according to the model for dendrite solidification of multicomponent alloys with unequal liquid diffusion coefficients. Predictions showed a good agreement with experimental data, especially for Al–5.3 at.% Zn master alloy with Mg contents from 5.5 to 6.5 at.%. Furthermore, solute concentration data was used to predict the maximun amount of τ phase precipitate in α-Al matrix which will impact positively in the electrochemical efficiency properties of Al–Zn–Mg alloys which will be employed for cathodic protection applications.

Keywords: Aluminium alloys; Solidification; Distribution of solute; Predictions; Sacrificial anode

1. Introduction

The as-cast microstructure of most solidified alloys consisted mainly of dendrites with eutectic between dendrite arms. To understand its behavior several dendrite growth models have been developed based on the steady state solution of the solidification problem involving a paraboloidal solid/liquid interface. The diffusion field ahead this interface has been given by the Ivantsov solution [1] and used to describe the growth of dendrites. Kurz et al. [2] based on the Ivantsov solution for the transport problem [3] and the marginal stability criterion [4], modeled the problem of constrained cellular or dendritic growth in the velocity range approaching that for absolute morphological stability. In addition, Gäumann and co-workers [5] considered the growth at the marginal stability and used the Ivantsov's model to determine the composition profile in the liquid ahead of the dendrite interface.

The modeling of solidification of ternary systems has been performed assuming independent diffusion of the solutes, such that the diffusion fields in ternary alloys are then given by similar mathematical functions as in binary systems and the boundary conditions at the solid/liquid interface given by the phase diagram. This approach has been applied to derive a dendrite growth model using the Ivantsov solution, the marginal stability criterion and independent solute diffusion [6]. Furthermore, by assuming no thermal gradient at the scale of the grain, negligible thermal undercooling, low growth rate, growth at the marginal stability limit, independent solute fields and neglect off-diagonal diffusion terms, it was developed a growth kinetic model for multicomponent dendrite tip [7]. Under those assumptions, the growth of the dendrite tip is governed by the supersaturation associated with the difference between the liquid concentration at the tip and far from the tip, normalized by the solute rejected by the tip. When the dendrite is growing at the marginal stability limit, the dendrite tip radius, dendrite tip concentration and dendrite tip undercooling for a multicomponent system are obtained.

This work present results of solute distribution (Zn + Mg) in α-Al dendrites of Al–Zn–Mg alloys and the results compared with predictions of the model of dendrite solidification of multicomponent alloys, and then, experimental results and predictions used to propose an appropriated alloy composition which can be used to produce Al alloys for cathodic protection applications of structures expose to marine environments against corrosion.

2. Prediction of solute distribution

In order to derive the distribution of solute Zn and Mg during dendrite solidification of Al–Zn–Mg alloys, it was employed the

* Corresponding author. Tel.: +52 56 22 54 89; fax: +52 56 16 13 71.
E-mail address: julioalb@servidor.unam.mx (J.A. Juarez-Islas).

0921-5093/$ – see front matter © 2005 Elsevier B.V. All rights reserved.
doi:10.1016/j.msea.2005.08.130

model for dendrite solidification of multicomponent alloys with unequal liquid diffusion coefficients developed by Rappaz and Boettinger [7], which is an extension of the model previously developed for columnar dendrite growth of ternary alloys [8]. During solidification of the alloy, a dendrite is developed and its tip is governed by the supersaturation:

$$\Omega_j = \frac{(C^*_{\mathrm{L},j} - C_{0,j})}{(C^*_{\mathrm{L},j} - C^*_{\mathrm{s},j})} = \left[\frac{(C^*_{\mathrm{L},j} - C_{0,j})}{C^*_{\mathrm{L},j}(1-k_j)}\right] = Iv(Pe_j) \quad (1)$$

where C^*_{L} is liquidus concentration at the solid/liquid interface, C_0 initial alloy concentration, C^*_{s} solidus concentration at the solid/liquid interface (in at.% or wt.%), $Iv(Pe)$ is Ivantsov number = $Pe\exp(Pe)E_1(Pe)$, where $E_1(Pe)$, the first exponential integral; Pe Péclet number = $VR/2D_{\mathrm{L}}$, V solidification growth velocity (m/s), R the dendrite tip radius (m) and D_{L} is the solute liquidus diffusion coefficient (m^2/s).

Assuming no thermal gradient at the scale of a grain, negligible thermal undercooling, low growth rate, growth at the marginal stability, independent solute fields given by the Ivantsov solution and neglect off-diagonal diffusion terms, the radius is expressed as:

$$R = 2\pi\left(\frac{\Gamma}{\sum_{j=1}^{n} m_j G_{\mathrm{c},j}}\right)^{1/2} \quad (2)$$

where Γ is capillarity constant (K m), m liquidus slope, G_{c} concentration gradient (wt.%/m or at.%/m) and $\pi = 3.1416$.

At the tip:

$$G_{\mathrm{c},j} = -\left(\frac{V}{D_{\mathrm{L}}}\right)(C^*_{\mathrm{L},j} - C^*_{\mathrm{s},j}) = -\left(\frac{V}{D_{\mathrm{L}}}\right)\left[\frac{C_{0,j}(1-k_j)}{1-(1-k_j)Iv(Pe_j)}\right] \quad (3)$$

where the partition coefficient $k = (C_{\mathrm{s}}/C_{\mathrm{L}})$.

By combining the equation corresponding to the dendrite tip radius and solute gradients at the tip, it is obtained the dendrite tip radius as a function of the Péclet number and from this, the solute concentration at the tip in the liquid as:

$$C^*_{\mathrm{L},j} = \frac{C_{0,j}}{1-(1-k_j)Iv(Pe_j)} \quad \text{for } j = 1, n \quad (4)$$

and as pointed out by Rappaz and Boettinger [7], if the undercooling of the alloy is small, all the parameters of the phase diagram can be estimated at the liquidus temperature of the alloy.

3. Experimental

Al–Zn–Mg alloys were obtained after placing Al, Zn and Mg elements of commercial purity (99.5%) into a high alumina crucible and melted under a vacuum induction furnace with a constant flux of argon and cast into an experimental arrangement as that shown in Fig. 1. Alloy composition of alloys was obtained by plasma spectroscopy and shown in Table 1.

Microstructure was revealed after grinding the specimens in emery paper wet with methanol instead of water to avoid corrosion of the specimens and electroetched in a solution containing 10% $HClO_4$ in ethanol and observed under a Stereoscan 440 scanning electron microscope. WDS microanalyses were performed on primary and secondary dendrite arms to determine the distribution of Zn and Mg elements. Microanalyses results were compared with predictions of solute distribution of Zn and Mg in α-Al solid solution according to the model of dendrite solidification of multicomponent alloys.

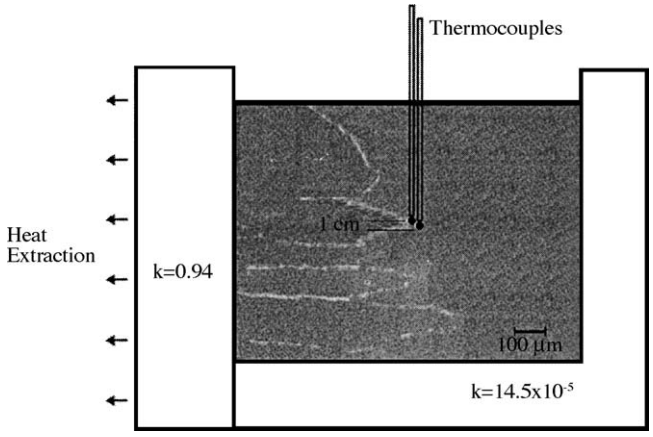

Fig. 1. Experimental arrangement used during solidification of Al-alloys (k in cal/(cm °C s)).

Table 1
Average alloy composition of samples

Elements	Basic			
	Anode 1	Anode 2	Anode 3	Anode 4
Mg	4.6 wt.%, 5.5 at.%	5.4 wt.%, 6.5 at.%	6.2 wt.%, 7.5 at.%	9.2 wt.%, 11.5 at.%
Zn	12.0 wt.%, 5.3 at.%			
Al	Balance			
	Traces			
Si	0.041–0.212 wt.%, 0.0426–0.2206 at.%			
Cu	0.22–0.92 wt.%, 0.10–0.50 at.%			
Fe	0.1 wt.%, 0.104 at.%			

The electrochemical behavior of Al-alloys was investigated in 3% NaCl solution. The electrochemical tests were carried out in a three-electrode cell arrangement. The samples of the Al-anode were put in a sample holder presenting an exposing area of 125 mm^2 to the electrolyte. A platinum gauge was used as a counter electrode and a saturated calomel electrode was employed as a reference electrode.

4. Results and discussion

The microstructure obtained after solidification of Al–Zn–Mg alloys is shown in Fig. 2 and consisted mainly of α-Al dendrites with small precipitates ($<2.0 \pm 0.3$ μm, shown by an arrow) of the τ phase on it and eutectic in interdendritic regions. As the Mg content increases, the volume percent of τ phase in α-Al matrix and the eutectic in interdendritic regions

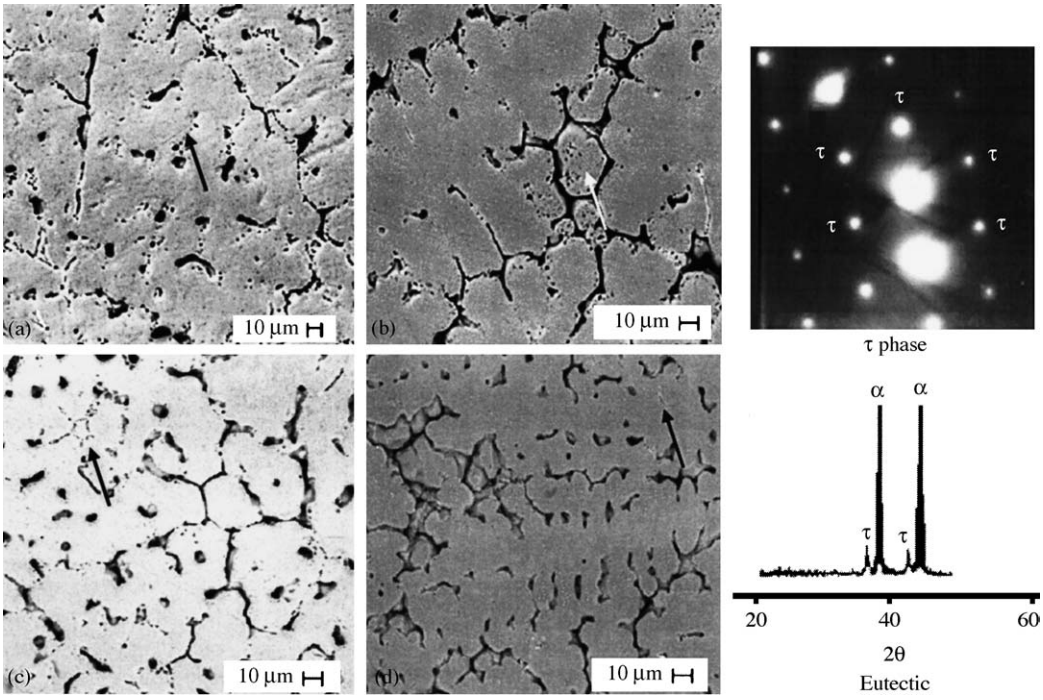

Fig. 2. SEM-microstructure of Al–5.3 at.% Zn master alloy (a) 5.5 at.% Mg, (b) 6.5 at.% Mg, (c) 7.5 at.% Mg and (d) 11.5 at.% Mg (arrows shows location of the intermetallic τ in α-Al solid solution).

reached a maximun of 2.25 and 15.8, respectively. Primary dendritic arm spacing decreased from 175 μm (5.5 at.% Mg) to 70 μm (11.5 at.% Mg), as is shown in Table 2.

At this point, it is important to mention that although the Al–Zn–Mg alloys (series 7*xxx*) has been widely studied due to the excellent mechanical properties reached after age hardening [9], because of the precipitation which occurs through a complex sequence of formation of Guinier–Preston (GP) zones during the decomposition of the supersaturated α-Al solid solution [10], involving the metastable η′ phase and the stable η phase, and as a result of the combination of both low density and high strength have made Al-alloys the primary material to be used in the aircraft and automotive industries.

Recently, it has been pointed out the Al–Zn–Mg system as a potential candidate to be used as an alloy for cathodic protection of extructures expose to marine environments, paying special attention to the effect of the τ phase in α-Al solid solution, to promote a good surface activation of the anode, avoiding the formation of the continuous, adherent and protective oxide film on the alloy surface once in service [11]. For this purpose, it is important to know the distribution of element Zn and Mg in α-Al solid solution and the capability of decomposition of the α-Al solid solution to precipitate the τ phase on it, in both as-solidified and as-heat-treated conditions.

Table 2
Volume percent of phases and dendrite arm spacing in samples

Anode	τ in α-Al matrix (vol.%)	Eutectic in interdendritic regions (vol.%)	λ_1 (μm)
1	0.70	10.0	175 ± 12.1
2	1.17	11.9	130 ± 9.2
3	1.74	15.2	85 ± 6.5
4	2.25	15.8	70 ± 3.3

Fig. 3 shows results of quantification and distribution of elements Zn + Mg in the α-Al solid solution, as detected by scanning electron microscopy microanalysis (WDS). As can be observed, microanalyses were performed in primary (λ_1) and secondary (λ_2) dendritic arms. For instance, the results showed that the amount of Zn + Mg retained in primary dendrite arms in the alloys under study varied from 6.5 to 6.8 at.%, while in secondary dendrite arms, the amount of Zn + Mg retained in α-Al solid solution varied depending of the location where the microanalyses were done. And as was noticed, the maximum amount of Zn + Mg retained in λ_2 reached at maximum value of 10.1 at.%, which is close to the maximum concentration of solute Zn + Mg at equilibrium [12].

Regarding prediction of solute distribution during solidification of Al–Zn–Mg alloys, it was calculated the distribution of Zn + Mg in α-Al during dendrite solidification, according to the model for dendrite solidification of multicomponent alloys with unequal liquid diffusion coefficients. For this purpose, the vertical section at constant 5.3 at.% Zn of the ternary Al–Zn–Mg phase diagram (Fig. 4) was employed to derive the values of $m_L = -3.93$ K/at.% and $k = 0.141$, for the L + α region, and $m_L = -1.45$ K/at.% and $k = 0.687$ for the L + α + τ region. Diffusion coefficients $D_{L,Zn} = 8.8 \times 10^{-8}$ m^2/s and $D_{L,Mg} = 9.45 \times 10^{-9}$ m^2/s were taken from refs. [13,14], and capillarity constants $\Gamma_{Mg} = 1.52 \times 10^{-7}$ K m and $\Gamma_{Zn} = 9.87 \times 10^{-7}$ K m were derived from the thermodynamic data for the Al–Mg–Zn system reported by Liang and Chang [15]. All these data, together with an experimental temperature gradient, $G_L = 500$ K/m were fed into Eq. (4). An example of the calculation is shown in Table 3 for the

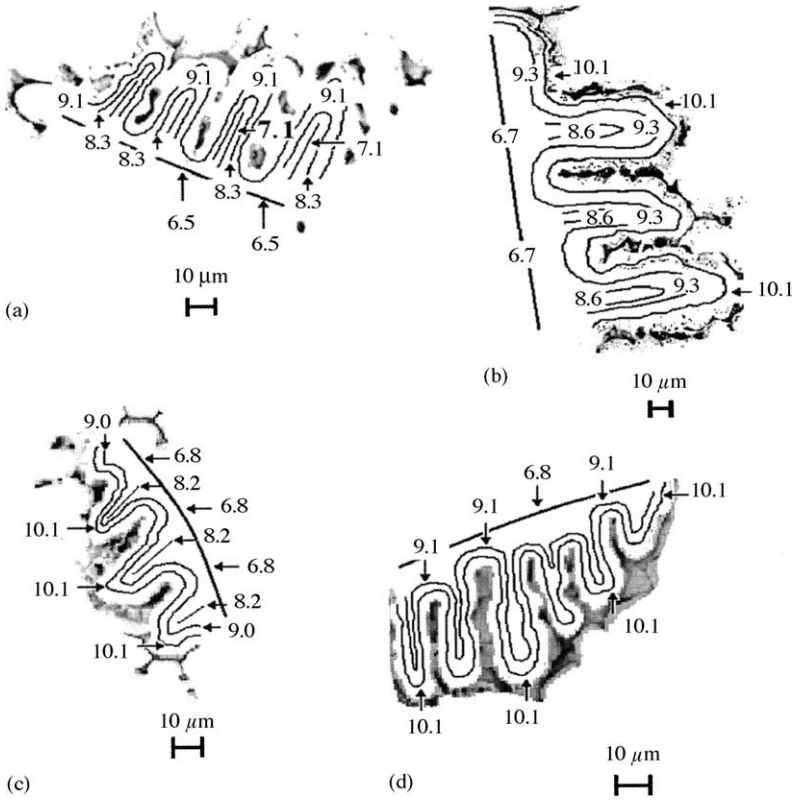

Fig. 3. Distribution of solute Zn + Mg in primary and secondary dendrite arm: (a) Al–5.3 at.% Zn–5.5 at.% Mg, (b) Al–5.3 at.% Zn–6.5 at.% Mg, (c) Al–5.3 at.% Zn–7.5 at.% Mg and (d) Al–5.3 at.% Zn–11.5 at.% Mg.

Al–5.3 at.% Zn–6.5 at.% Mg alloy, including predictions to solidification growth velocities up to the absolute stability limit, where the amount of solute retained in solid solution goes to C_0.

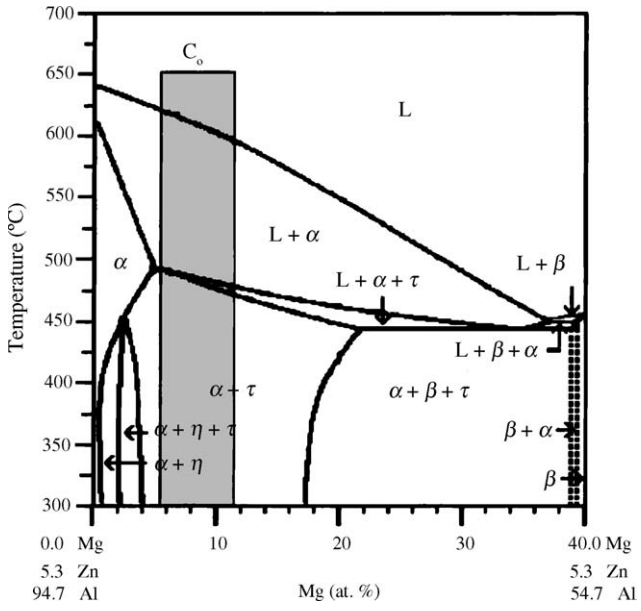

Fig. 4. Vertical section at constant 5.3 at.% Zn of the ternary Al–Zn–Mg phase diagram where it is shown by a vertical bar, the alloy composition of interest [14].

Details of prediction of solute concentration C_L^* and C_s^* are shown in Fig. 5, where the broken horizontal lines corresponded to prediction of solute concentration (Zn + Mg) for the L + α region, while the full horizontal lines corresponded to prediction of solute concentration (Zn + Mg) for the L + α + τ region for solidification growth velocities between 5×10^{-4} and 10×10^{-4} m/s. These velocities comprise the experimental growth velocity of 6.5×10^{-4} m/s (full vertical line) reached during the experiments. The full circles represented either the amount of Zn + Mg retained in λ_1 or λ_2 and the open square indicated the experimental average solute Zn + Mg concentration detected by WDS-microanalysis in the all dendrite. As can be observed, for Mg concentrations between 5.5 and 6.5 at.% Mg, predictions are in agreement with experimental results and when the amount of Mg increases, the agreement is getting poor. This can be explained because the mathematical model employed for predictions considered the growth kinetics of a dendrite at low velocity [7,8] to describe the growth of a dendrite grain. The difference between previous models [16,17] is the consideration of average concentration of the interdendritic liquid region which is different from the tip concentration and necessary when the multicomponent alloy has unequal liquid diffusion coefficients. However, the model did not take into account back diffusion or the effect of eutectic growth in interdendritic regions [11], which have an impact on predictions as C_0 increases as shown in Fig. 5.

Prediction of solute concentration in α-Al as a function of solidification growth velocity during solidification of the alloy is a useful tool to be considered during alloy design. For instance,

Table 3
Distribution of solute Zn and Mg for the (a) L + α region and (b) L + α + τ region for the Al–5.3 at.% Zn–6.5 at.% Mg alloy

V_S (m/s)	$C^*_{s,Zn}$ (at.%)	$C^*_{s,Mg}$ (at.%)	$C^*_{s,Zn+Mg}$ (at.%)	$C^*_{L,Zn}$ (at.%)	$C^*_{L,Mg}$ (at.%)	$C^*_{L,Zn+Mg}$ (at.%)
(a) L + α						
1×10^{-4}	0.806	1.068	1.874	5.714	7.574	13.288
5×10^{-4}	0.820	1.162	1.982	5.816	8.241	14.057
1×10^{-3}	0.830	1.250	2.080	5.890	8.856	14.746
5×10^{-3}	0.871	1.425	2.296	6.178	10.110	16.288
1×10^{-2}	0.899	1.550	2.449	6.374	10.972	17.346
5×10^{-2}	0.999	1.934	2.933	7.076	13.714	20.790
1×10^{-1}	1.060	2.156	3.216	7.518	15.290	22.808
5×10^{-1}	1.265	2.838	4.103	8.969	20.131	29.100
1×10^{0}	1.384	3.232	4.616	9.820	22.920	32.740
5×10^{0}	1.772	4.608	6.380	12.563	32.680	45.243
$V_{ab} = 23.8$	5.300	6.500	11.800	37.580	46.010	83.590
(b) L + α + τ						
1×10^{-4}	3.778	4.905	8.683	5.500	7.139	12.639
5×10^{-4}	3.832	5.150	8.982	5.579	7.491	13.070
1×10^{-3}	3.870	5.275	9.145	5.634	7.679	13.313
5×10^{-3}	4.000	5.622	9.622	5.824	8.184	14.008
1×10^{-2}	4.078	5.790	9.868	5.935	8.430	14.365
$V_{ab} = 0.656$	5.300	6.500	11.800	7.715	9.461	17.176

in the alloys under study, predictions of solute Zn + Mg for the region L + α + τ were close to those determined experimentally, specially for Mg concentrations <7.0 at.%. The knowledge of the amount of solute retained in solid solution, can be use to predict the maximum fraction of precipitates that form during aging. For this aim, Bjorneklett et al. [18] and Liu et al. [19] have proposed relationships to predict the maximum fraction of precipitates that form during aging as a function of the mean solute concentration of the alloy, of the form:

$$\Delta f_p = k_1[C_m - C_m^0]^3 \quad (5)$$

where k_1 is a constant equal at 0.1399 vol.%/at.%^{3} for Al–Zn–Mg alloys, C_m the mean solute concentration in the matrix and C_m^0 the matrix solute content in stabilized base material. According to Eq. (5) the maximum fraction of precipitates of τ phase that form after heat treatment of the alloys under study will be ∼5.94 vol.% which is close to the value of 5.5 vol.% obtained experimentally. Promoting the precipitation of this τ

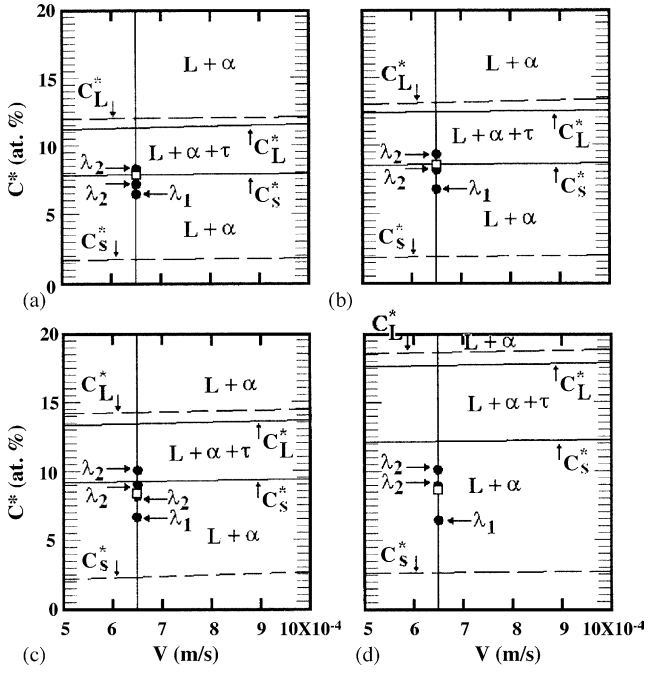

Fig. 5. Prediction versus experimental results for Al–5.3 at.% Zn master alloy with additions of (a) 5.5 at.% Mg, (b) 6.5 at.% Mg, (c) 7.5 at.% Mg and (d) 11.5 at.% Mg. The broken horizontal lines corresponded to C^*_L and C^*_s concentrations (Zn + Mg) for the L + α region and the full horizontal lines corresponded to C^*_L and C^*_s concentrations (Zn + Mg) for the L + α + τ region. The vertical line represent the growth rate achieved during the experiments. The symbol (□) represents the average Zn + Mg content in the dendrite, the symbol (●) represents the concentration Zn + Mg in the primary (λ_1) or secondary (λ_2) dendrite arms.

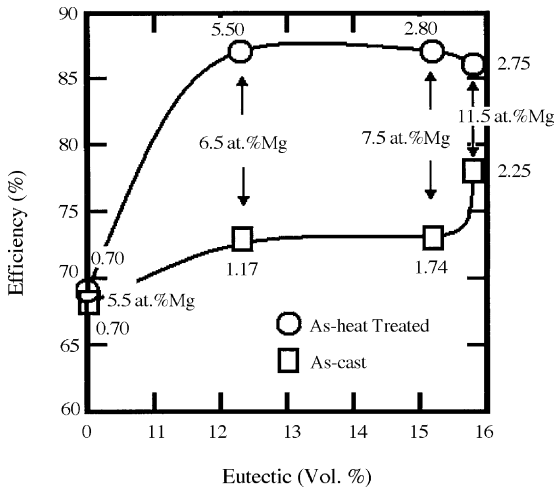

Fig. 6. Plot of efficiency as a function of the euctectic and intermetallic content. Symbols (○) and (□) represent the amount of τ-intermetallic in α-Al matrix in the as-cast and heat-treated condition, respectively.

phase in the α-Al solid solution increased the electrochemical properties of the alloys, as shown in Fig. 6.

5. Conclusions

1. Distribution of solute Zn + Mg during dendrite solidification of Al alloys, according to the model for dendrite solidification of multicomponent alloys with unequal liquid diffusion coefficients showed a good agreement with experimental results for Zn + Mg contents <7.0 at.%. As the Mg content increase, the agreement is poor due to the model did not take into account the presence of eutectic and the effect of back diffusion.
2. Predictions of C_s^* as a function of growth rate carried out in the L + α + τ region were used to predict the volume fraction of τ phase formed after heat treatment, predicting a maximum of 5.94 vol.%, similar to that obtained experimentally in the alloys under study.
3. Quantification and prediction of solute distribution allow to select the Al–5.3 at.% Zn–6.5 at.% Mg as a potential candidate to be used as an alloy for cathodic protection applications of structures expose to marine environments against corrosion.

Acknowledgments

The authors acknowledge the financial support from DGAPA with grant IN102601 and CONACYT with grants NC-204 and 45453Y. We also thank Mr. Caballero for carrying out the photographic work.

References

[1] G.P. Ivantsov, Dok. Akad. Nauk. 58 (1947) 567–572.
[2] W. Kurz, B. Giovanola, R. Trivedi, Acta Metall. 34 (1986) 823–830.
[3] H. Esaka, W. Kurz, J. Cryst. Growth 69 (1984) 362–366.
[4] J.S. Langer, H. Muller-Krumbhaar, Acta Metall. 26 (1978) 1681–1687.
[5] W. Kurz, M. Gäumann, R. Trivedi, Mater. Sci. Eng. A A226 (1997) 763–769.
[6] M. Bobadilla, J. Lacaze, G. Lesoult, J. Cryst. Growth 89 (1988) 531–544.
[7] M. Rappaz, W.J. Boettinger, Acta Mater. 47 (1999) 3205–3219.
[8] M. Rappaz, S.A. David, J.M. Viutek, L.A. Boatner, Metall. Trans. 21A (1990) 1753–1766.
[9] J. Lendvai, Mater. Sci. Froum. 217–222 (1996) 43–56.
[10] X.J. Jiang, B. Noble, B. Holme, G. Waterloo, J. Tafto, Metall. Mater. Trans. A 31A (2000) 339–348.
[11] C. Gonzalez, O. Alvarez, J. Genesca, J.A. Juárez-Islas, Metall. Mater. Trans. A 34A (2003) 2991–2997.
[12] D.A. Petrov, in: G. Petzow, G.E. Effemberg (Eds.), Ternary Alloys, vol. 3, VCH Weinheim, Germany, 1986, p. 57.
[13] N.L. Peterson, S.J. Rothman, Phys. Rev. B: Solid State 1 (1970) 3264–3273.
[14] B.V. Deryagin, R.M.B.V. Deryagin, Zh. Tekh. Fiz. 18 (1984) 1443–1448.
[15] H. Liang, Y.A. Chang, Metall. Mater. Trans. A 28A (1997) 1725–1734.
[16] M. Rappaz, Ph. Thévoz, Acta Metall. 35 (1987) 1487–1497.
[17] M. Rappaz, Ph. Thévoz, Acta Metall. 35 (1987) 2929–2933.
[18] B.J. Bjorneklett, O. Grong, O.R. Myhr, A.O. Klñuken, Metall. Mater. Trans. A 30A (1999) 2667–2677.
[19] G. Liu, G.J. Zhang, X.D. Ding, J. Sun, K.H. Chen, Mater. Sci. Eng. A 34A (2003) 113–124.